ac Stark Splitting and Quantum Interference with Intersubband Transitions in Quantum Wells

J. F. Dynes,[1] M. D. Frogley,[1] M. Beck,[2] J. Faist,[2] and C. C. Phillips[1]

[1]*Experimental Solid State Group, Department of Physics, Imperial College London, London SW7 2BZ, United Kingdom*

[2]*Institute of Physics, University of Neuchâtel, CH-2000 Neuchâtel, Switzerland*

(Received 5 November 2004; published 22 April 2005)

Resonant optical coupling experiments have demonstrated coherent quantum interference between the Stark-split ''dressed states'' of a synthesized 3-level electronic system in a semiconductor quantum well. Analysis of the dephasing mechanisms reveals dipole selection rules closely analogous to those seen in atomic spectroscopy experiments. In this respect, these systems behave as ''artificial atoms'' for the purposes of observing a range of nonclassical coherent optical effects. The prospects for exploiting them for scalable quantum information processing applications are more promising than previous dephasing models would have predicted.

DOI: 10.1103/PhysRevLett.94.157403 PACS numbers: 78.67.De, 03.67.Lx, 42.50.Hz, 63.20.Ls

When a two-level electronic system is resonantly ($\hbar\omega = E_{12}$) excited with a weak optical field its response is normally described with a perturbative ''Fermi's golden rule'' treatment to compute the absorption and the spontaneous and stimulated transition rates. At higher intensities perturbative treatments of increasing order suffice, but these fail when the optical coupling energy (characterized by the Rabi frequency, $\Omega_{12} = ez_{12}E/\hbar$, where ez_{12} is the dipole matrix element and E is the optical electric field amplitude) approaches the linewidth of the transition. The system now becomes ''dressed'' into new mixed electron-photon eigenstates [1]which are given by

$$|a\rangle = 1/\sqrt{2}(|1, n+1\rangle + |2, n\rangle),$$
$$|b\rangle = 1/\sqrt{2}(|1, n+1\rangle - |2, n\rangle, \quad (1)$$

where n is the photon number.

Viewed in the frequency domain, the ac optical field has Stark split the ''bare'' states $|1\rangle$ and $|2\rangle$ into doublets, of energy separation $\hbar\Omega_{12}$. In the time domain the electron population is found to cycle coherently between the two bare states with a period, $2\pi/\Omega_{12}$, which is less than the dephasing time.

These dressed states have the advantage that their quantum mechanical *phases* can be controlled and probed optically. It now becomes possible to observe quantum interference (QI) between the transition *amplitudes* (so-called matter-wave interference), even within a single quantum oscillator. In atomic spectroscopy this has a number of nonclassical manifestations, such as Autler-Townes splitting [2], electromagnetically induced transparency (EIT) [3], and lasing without inversion [4]. More recently such systems have attracted interest as candidate ''qubits'' for implementing quantum data processing and communication schemes.

Practical applications favor a scalable solid-state system, but the resonant nature of QI requires a peaked absorption spectrum which is rarely seen in solids. Nevertheless, EIT has been reported, using electron subbands [5] and interband excitons [6], in spite of the fast ($\sim$ psec^{-1}) dephasing rates [5,7].

Intersubband transitions (ISBT's), between the states of an electron confined in a semiconductor quantum well, are particularly attractive for these studies [8]. Strong electron-electron interactions [9] produce a collective oscillation, which can behave as a single quantum object, and whose large ($z_{ij} \sim$ nm) dipoles result in Rabi frequencies which are large enough to overcome dephasing. ISBT energies, wave function symmetries, and absorption strengths can also be controlled with a flexibility unknown in natural atoms, and this has recently attracted theoretical and experimental attention [10].

Here we report the first observation of ac Stark splitting of an ISBT in a semiconductor quantum well. Furthermore, we show that the ISBT dephasing mechanisms have characteristics which make them behave essentially as ''artificial atoms.'' This has allowed the clear observation of matter-wave quantum interference.

The system studied is a 3-level ''cascade'' ISBT scheme [Fig. 1(a)], which allows the dressing of the $|1\rangle \rightarrow |2\rangle$ electronic transition to be probed via the extra absorption features it produces in a distinctly different ($\hbar\omega \sim E_{23}$) spectral region.

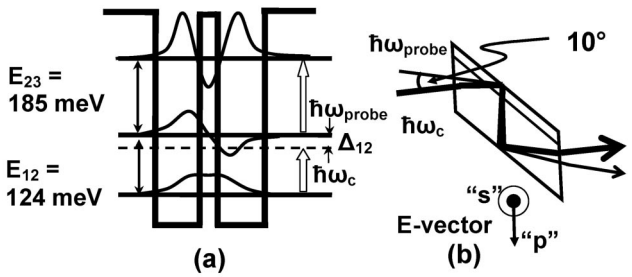

FIG. 1. (a) Schematic of the 3-level cascade electronic system synthesized in a semiconductor quantum well. ω_c and ω_{probe} are the coupling and probe beam optical frequencies and Δ_{12} is the detuning between the coupling beam and the $|1\rangle \rightarrow |2\rangle$ transition. (b) Experimental coupling geometry.

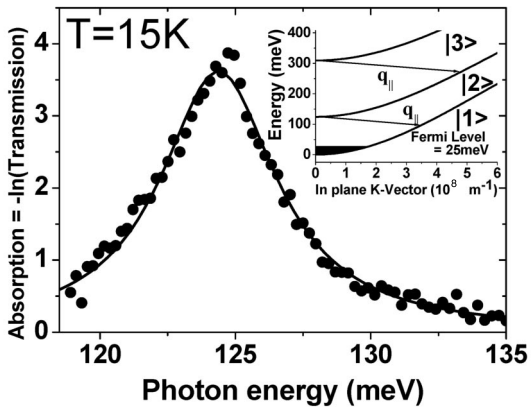

FIG. 2. Linear absorption spectrum of the $|1\rangle - |2\rangle$ transition in the absence of the coupling field. Linewidth = 5.2 meV ± 3%. Closed circles, experimental data; solid line, Lorentzian fit. Inset: Calculated [12] in-plane wave vector dispersion curves. The $q_{\|}$ denote the optical phonon wave vectors involved in population decay.

The experiments use two synchronized, independently tunable trains of ~100 ps wide pulses from a parametric midinfrared laser system [11]. Both beams are focused through a 300 μm diameter pinhole into the sample. The "coupling" pulse intensity reaches ~5 MW/cm^2, but the "probe" pulse is kept ~1000 times weaker to ensure linearity in the measured absorption spectra. The beams are separated by 10° to aid discrimination, and both are sufficiently spectrally narrow for measurements to be effectively monochromatic.

The sample consists of 30 periods, each with a 4.8 nm $In_{0.47}Ga_{0.53}As$/ 0.2 nm $Al_{0.48}In_{0.52}As$/ 4.8 nm $In_{0.47}Ga_{0.53}As$ coupled quantum well, separated by modulation-doped 36 nm $Al_{0.48}In_{0.52}As$ barriers. The undoped InP substrate is polished into a 45° rhomb [Fig. 1(b)] so that absolute absorption data can be obtained by ratioing spectra from s- and p-polarized laser pulses, as only the latter couple to the ISBT. Integrating the linear $\sim E_{12}$ Lorentzian absorption spectrum [Fig. 2] gives the sheet electron density as 4.7×10^{11} cm^{-2} (±10%), corresponding to a Fermi energy (Fig. 2 inset) 25 meV above the minimum of state $|1\rangle$.

The bare state transition energies were measured as $E_{12} = 124$ meV (Fig. 2) and, from a separate induced absorption measurement (not shown), $E_{23} = 185$ meV, implying $E_{13} = 309$ meV. The corresponding transition dipoles were calculated, with an 8-band nonparabolicity method [12], as $z_{12} = 2.335$ nm, $z_{23} = 2.341$ nm, and $z_{13} = 0.120$ nm.

Using resonant ($\hbar\omega_c = E_{12} = 124$ meV) coupling pulses, the lowest coupling pulse intensities produce a weak Lorentzian induced absorption peak centered at $E_{23} = 185$ meV with 5 meV full width at half maximum (FWHM). As the coupling pulse intensity is increased this "power broadens" to ~8 meV FWHM [Fig. 3(a)] by the

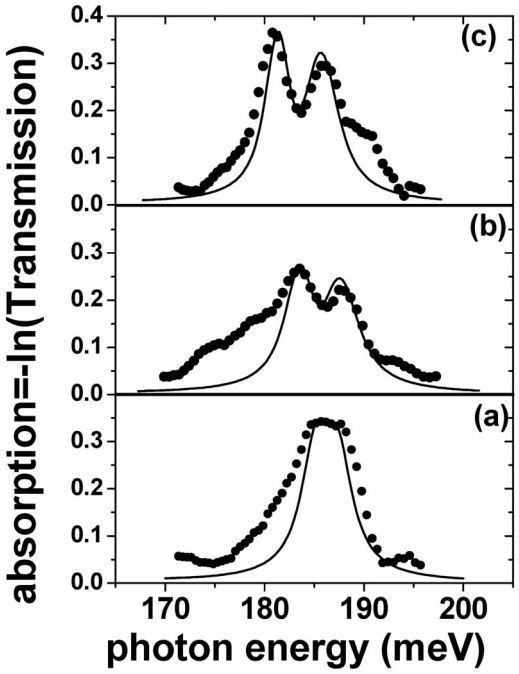

FIG. 3. Induced absorption spectra, in the vicinity of E_{23}, in the presence of a coupling pulse resonant ($\hbar\omega_c = E_{12} =$ 124 meV) with the E_{12} transition. Coupling intensities correspond to Rabi energies ($\hbar\Omega_{12}$) of (a) 2 meV, (b) 3 meV, and (c) 4 meV. Full circles, experimental data; solid lines, predictions of the density matrix calculation (corrected for the spatiotemporal pulse profiles) with γ_{13} set to 0.9 meV.

time $\hbar\Omega_{12}$ reaches 2.0 meV. At higher $\hbar\Omega_{12}$ values an increasingly well-resolved doublet structure appears [Figs. 3(b) and 3(c)]. The splitting energy scales with the square root of the coupling pulse intensity [Fig. 4], characteristic of an ac Stark-splitting mechanism. Importantly, at high $\hbar\Omega_{12}$ values, the split peaks have linewidths

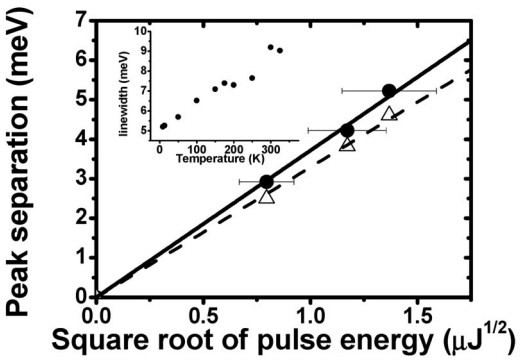

FIG. 4. Dependence of peak splitting on resonant-coupling pulse energy. Filled circles/solid line, experimental data; open triangles/dashed line, predictions of the density matrix model with spatiotemporal averging. The lines are guides to the eye. Inset: temperature dependence of the small-signal linewidth of the $|1\rangle - |2\rangle$ transition.

(~3 meV FWHM) which are significantly less than the 5 meV homogeneous linewidth of the bare E_{23} transition from which they evolved.

To model these results to full order in coupling field intensity, we employ the following density matrix:

$$\frac{\partial \rho_{11}}{\partial t} = \gamma_2 \rho_{22} + i\Omega_{12}(\rho_{12} - \rho_{21}),$$

$$\frac{\partial \rho_{22}}{\partial t} = -\gamma_2 \rho_{22} + \gamma_3 \rho_{33} - i\Omega_{12}(\rho_{12} - \rho_{21}) + i\Omega_{23}(\rho_{23} - \rho_{32}),$$

$$\frac{\partial \rho_{33}}{\partial t} = -\gamma_3 \rho_{33} - i\Omega_{23}(\rho_{23} - \rho_{32}),$$

$$\frac{\partial \rho_{12}}{\partial t} = (i\Delta_{12} - \gamma_{12}/2)\rho_{12} - i\Omega_{12}(\rho_{22} - \rho_{11}) + i\Omega_{23}\rho_{13},$$

$$\frac{\partial \rho_{13}}{\partial t} = (i\Delta_{13} - \gamma_{13}/2)\rho_{13} - i\Omega_{12}\rho_{23} + i\Omega_{23}\rho_{12},$$

$$\frac{\partial \rho_{23}}{\partial t} = (i\Delta_{23} - \gamma_{23}/2)\rho_{23} - i\Omega_{23}(\rho_{33} - \rho_{22}) - i\Omega_{12}\rho_{13}.$$

$$\rho_{ij} = \rho_{ji}^{*} \quad and \quad \sum_{i=1}^{3} \rho_{ii} = 1$$

where Ω_{ij} are the Rabi frequencies for the $|i\rangle - |j\rangle$ transitions. The detuning parameters are defined as $\Delta_{ij} = E_{ij} - \hbar\omega_c$ and $\Delta_{31} = \Delta_{12} + \Delta_{23}$ is the two photon detuning. The formalism is similar to the established treatment [13] for 3-level atoms, save for the extra Ω_{ij} terms which have been added to allow for the coupling field simultaneously dressing more than one transition [5]. Solving for steady-state solutions and employing the quantum regression theorem [13] gives small-signal absorption spectra comprising all the excitations of the coupled electron-photon system. The optical pulses have known spatiotemporal profiles which change slowly enough (~10 psec) to be followed adiabatically by the ISBT coherences. This allows us to produce a suitably weighted sum of absorption spectra (corresponding to different coupling intensities) for direct comparison with the experiment.

Dephasing processes enter this calculation phenomenologically, via the population decay (γ_i) and transition dephasing (γ_{ij}) parameters. For isolated natural atoms both are determined by radiative coupling to isotropic photon modes, and can be readily estimated, but with ISBT's dephasing is via coupling to the lattice phonon spectrum and via interface roughness scattering (IRS); both of these require careful analysis. The dominant phonon contributions come from piezoelectric and Frohlich coupling to acoustic and optical phonon branches, respectively. Because, in both cases, the ISBT couples via the phonon's oscillating *electric* field [14], the rates scale with z_{ij}^2, just as with natural atoms.

However, the phonon dispersion characteristics lead to population decay rates (γ_i) which are dominated by the inelastic emission of longitudinal optical (LO) phonons, at a rate which scales as $[z_{i,i-1}/q_{\|}]^2$, where $q_{\|} \sim [2m^*(E_{i,i-1} - \hbar\omega_{\mathrm{LO}})/\hbar^2]^{1/2}$ is the appropriate phonon wave vector (Fig. 2 inset), and $\hbar\omega_{\mathrm{LO}} \sim 34$ meV is the InGaAs LO phonon energy. Piezoelectric scattering has a similar $1/q^2$ dependence [14], albeit modified by electron screening. The scattering rate peaks for acoustic phonons with wave vectors close to q_0, the Thomas-Fermi screening wave vector. Because these phonons have low energies (~1 meV in this case [15]), this mechanism is routinely ignored in, e.g., electron energy and momentum relaxation calculations, but the scattering *rates* are nonetheless high, making it the dominant phonon dephasing mechanism [14]. Our wave function modeling shows that fluctuations in the central 0.2 nm AlInAs barrier thickness make the dominant IRS contributions and that these are similar for γ_{12} and γ_{23} but are some >35 times weaker for γ_{13}.

Accordingly, we write $\gamma_{12} = \gamma_2 + \gamma^{\mathrm{dph}}{}_{12}$, $\gamma_{23} = \gamma_2 + \gamma_3 + \gamma^{\mathrm{dph}}{}_{23}$, and $\gamma_{13} = \gamma_3 + \gamma^{\mathrm{dph}}{}_{31}$, where the $\gamma^{\mathrm{dph}}{}_{i,j}$ comprise the sum of the quasielastic acoustic phonon scattering and the elastic IRS, both of which dephase the transitions without depopulating them, akin to atomic collisional broadening in gases. The temperature dependence of the ISBT linewidth (Fig. 4 inset) indicates that IRS contributes 40%–60% of the dephasing [16] in these measurements.

A separate absorption saturation intensity measurement [17] gives the population decay rate of the $|1\rangle - |2\rangle$ transition as $\gamma_2 \sim 1.3$ meV, and we then use the above scaling arguments to set $\gamma_3 \sim 0.9$ meV. We can measure $\gamma_{12} \sim \gamma_{23} = 5$ meV, but γ_{13}, the only remaining parameter, concerns a transition which is practically dipole forbidden, and is anyway outside the laser tuning range. A full phonon scattering rate calculation is outside the scope of this Letter, but as a working approximation we assume that the acoustic phonon dephasing is dominated by the same $q \sim q_0$ phonons for all three transitions. The above arguments then imply that both the phonon and IRS contributions to $\gamma^{\mathrm{dph}}{}_{13}$ are negligible (< 0.03%) compared with the other two transitions, and hence that $\gamma_{13} \sim \gamma_3 \sim 0.9$ meV.

These arguments generate dephasing terms which are in ratios closely analogous to those of radaitively dephasing isolated natural atoms. They imply that, for the purposes of designing and exploiting coherent optical effects, ISBT's can be most usefully thought of as "artificial atoms." In contrast if, as has been done in the past, a simpler "level broadening" approximation is used, the measured linewidths imply that each level is ~2.5 meV wide and hence that $\gamma_{ij} = 5$ meV for all three ISBT transitions.

The solid curves in Fig. 3, modeled with the "artificial atom" dephasing values, closely reproduce the observed peak splittings, the peak narrowing due to quantum interference effects, and the absolute absorption coefficients. Figure 5(b) compares the predictions of the artificial atom and the level broadening pictures. The latter clearly over-

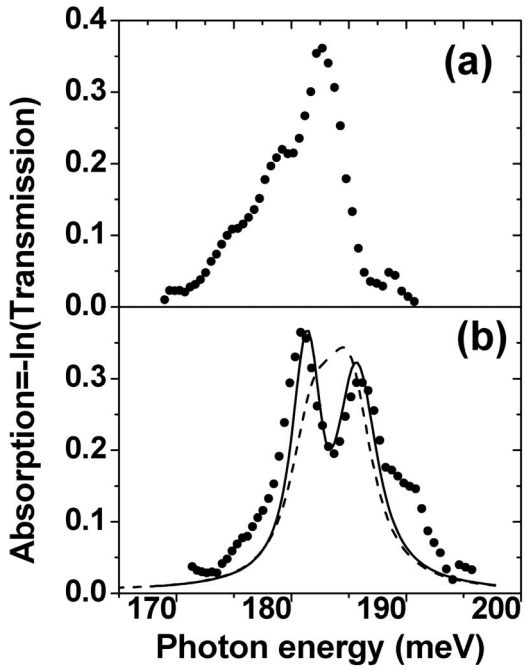

FIG. 5. (a) Measured induced absorption spectra with a nonresonant-coupling beam ($\hbar\omega_c = 134$ meV), tuned 10 meV above E_{12}. (b) Comparison between the $\hbar\Omega_{12} = 4$ meV resonant-coupling experiment (full circles) and the density matrix model using the artificial atom arguments ($\gamma_{13} = 0.9$ meV, solid line) and the level broadening argument ($\gamma_{13} = 5$ meV, dashed line).

estimates the γ_{13} dephasing rate, to the point where both peak-splitting and quantum interference effects are completely obscured. Figure 5(a) confirms the coherent nature of the experiment; detuning the coupling beam below the E_{12} resonance, by an amount (10 meV) larger than the natural linewidth (5 meV), produces only small (1–2 meV) perturbative shifts and an asymmetric line shape for the induced $|2\rangle - |3\rangle$ transition.

Note that the doublet in Fig. 3(c) cannot arise from a ''spectral-hole-burning'' mechanism because it appears at energy completely different from the coupling beam. At high levels of resonant excitation, carrier heating populates [17] high $\mathbf{k}_\parallel$ states (up to $\mathbf{k}_\parallel \sim 3 \times 10^8$ m^{-1}), whereupon subband nonparabolicity starts to weaken the ''single oscillator'' nature of the ISBT [9], particularly at intermediate Rabi frequencies, and for off-resonant driving conditions. This results in the appearance of absorption $\sim$10 meV below E_{23} [Fig. 3(b)]. Nevertheless, at $\Omega_{12} \sim$ 4 meV, we find that $>$90% of the electron population is participating in coherent Rabi oscillations between states $|1\rangle$ and $|2\rangle$.

In conclusion, we have observed dynamic Stark splitting of the ground and first excited states of a quantum well system, and clear signatures of coherent ''matter-wave'' interference. Density matrix modeling clearly indicates that artificial atom dephasing models are needed to explain these observations.

This work was supported by the UK Engineering and Physical Sciences Research Council. Useful discussions with E. Paspalakis are gratefully acknowledged.

[1] S. E. Harris, Phys. Rev. Lett. **64**, 1107 (1990); P. L. Knight, Comments At. Mol. Phys. **15**, 193 (1984); M. O. Scully and M. S. Zubairy, *Quantum Optics* (Cambridge University Press, Cambridge, England, 1997).
[2] S. H. Autler and C. H. Townes, Phys. Rev. **100**, 703 (1955).
[3] K.-J. Boller, A. Imamoglu and S. E. Harris, Phys. Rev. Lett. **66**, 2593 (1991); J. E. Field, K. H. Hahn, and S. E. Harris, Phys. Rev. Lett. **67**, 3062 (1991).
[4] A. S. Zibrov *et al.*, Phys. Rev. Lett. **75**, 1499 (1995); G. Padmabandu *et al.*, Phys. Rev. Lett. **76**, 2053 (1996).
[5] G. B. Serapiglia *et al.*, Phys. Rev. Lett. **84**, 1019 (2000).
[6] M. C. Phillips *et al.*, Phys. Rev. Lett. **91**, 183602 (2003); M. Saba *et al.*, Phys. Rev. B **62**, R16 322 (2000).
[7] R. A. Kaindl *et al.*, Phys. Rev. Lett. **80**, 3575 (1998).
[8] D. Frohlich, R. Wille, W. Schlapp, and G. Weimann, Phys. Rev. Lett. **59**, 1748 (1987).
[9] D. E. Nikonov, A. Imamoglu, L. V. Butov, and H. Schmidt, Phys. Rev. Lett. **79**, 4633 (1997); D. E. Nikonov and A. Imamoglu, Phys. Rev. B **59**, 12 212 (1999); P. M. Alsing, D. H. Huang, D. A. Cardimona, and T. Apostolova, Phys. Rev. A **68**, 033804 (2003); J. Li and C. Z. Ning, Phys. Rev. Lett. **91**, 097401 (2003).
[10] S. M. Sadeghi, S. R. Leffler, and J. Meyer, Phys. Rev. B **59**, 15 388 (1999); H. Schmidt and A. Immamoglu, Opt. Commun. **131**, 333 (1996).
[11] K. L. Vodopyanov and V. Chazapis, Opt. Commun. **135**, 98 (1997); K. L. Vodopyanov, J. Opt. Soc. Am. B **16**, 1579 (1999).
[12] K. H. Yoo, L. R. Ram Mohan, and D. F. Nelson, Phys. Rev. B **39**, 12 808 (1989).
[13] L. M. Narducci *et al.*, Phys. Rev. A **42**, 1630 (1990).
[14] See, e.g., B. K. Ridley, *Quantum Processes in Semiconductors* (Clarendon Press, Oxford, 1988).
[15] Following Ref. [14], this dominant acoustic phonon energy is estimated as $(\hbar q_0)^2/8m^*$, where $q_0 = (e^2 n/\varepsilon_0 \varepsilon_r E_F)^{1/2}$ is the 3D Thomas-Fermi screening wave vector, n is the average 3D electron density, E_F is the Fermi energy in the lowest subband, and $m^* \sim 0.045 m_o$, the electron effective mass.
[16] The absorbed optical energy would normally warm the lattice by only $\sim$5 K. However, on these short time scales, the phonon distributions are likely to be strongly athermal with high occupation factors in the modes which are actually coupled to the ISBT's. We estimate that the mean effective phonon dephasing temperature rises by up to $\sim$150 K, making the appearance of the sharp features in Fig. 5 all the more remarkable.
[17] S. Slivken, V. I. Litvinov, M. Razeghi, and J. R. Meyer, J. Appl. Phys. **85**, 665 (1999); G. B. Serapiglia, K. L. Vodopyanov, and C. C. Phillips, Appl. Phys. Lett. **77**, 857 (2000).